

$\psi(2S)$ and $\Upsilon(3S)$ hadroproduction in the parton Reggeization approach: Yield, polarization, and the role of fragmentation

B. A.Kniehl,^{1,*} M. A.Nefedov,^{1,2,†} and V. A.Saleev^{1,2,‡}

¹*II. Institut für Theoretische Physik, Universität Hamburg,
Luruper Chaussee 149, 22761 Hamburg, Germany*

²*Samara National Research University,
Moscow Highway, 34, 443086, Samara, Russia*

Abstract

The hadroproduction of the radially excited heavy-quarkonium states $\psi(2S)$ and $\Upsilon(3S)$ at high energies is studied in the parton Reggeization approach and the factorization formalism of non-relativistic QCD at lowest order in the strong-coupling constant α_s and the relative heavy-quark velocity v . A satisfactory description of the $\psi(2S)$ transverse-momentum (p_T) distributions measured by ATLAS, CMS, and LHCb at center-of-mass energy $\sqrt{S} = 7$ TeV is obtained using the color-octet long-distance matrix elements (LDMEs) extracted from CDF data at $\sqrt{S} = 1.96$ TeV. The importance of the fragmentation mechanism and the scale evolution of the fragmentation functions in the upper p_T range, beyond 30 GeV, is demonstrated. The $\Upsilon(3S)$ p_T distributions measured by CDF at $\sqrt{S} = 1.8$ TeV and by LHCb at $\sqrt{S} = 7$ TeV and forward rapidities are well described using LDMEs fitted to ATLAS data at $\sqrt{S} = 7$ TeV. Comparisons of polarization measurements by CDF and CMS at large p_T values with our predictions consolidate the familiar problem in the $\psi(2S)$ case, but yield reasonable agreement in the $\Upsilon(3S)$ case.

PACS numbers: 12.38.Bx, 12.39.St, 12.40.Nn, 13.87.Ce

*Electronic address: kniehl@desy.de

†Electronic address: nefedovma@gmail.com

‡Electronic address: saleev@samsu.ru

I. INTRODUCTION

The production of heavy quarkonia at hadron colliders is a unique laboratory for studies of the interplay between the perturbative treatment of hard subprocesses and nonperturbative hadronization models. Thanks to the hierarchy $m_Q \gg \Lambda_{\text{QCD}}$, where m_Q is the mass of the heavy quark $Q = c, b$ and Λ_{QCD} is the asymptotic scale parameter of quantum chromodynamics (QCD), the nonrelativistic-QCD (NRQCD) factorization hypothesis [1] (see also the recent reviews in Ref. [2]) allows one to factorize the effects of short and long distances and to parametrize the latter in terms of a few long-distance matrix elements (LDMEs). While color-singlet (CS) LDMEs are calculable in potential models [3], the only way to extract color-octet (CO) LDMEs available so far is to fit them to experimental data. This implies that, to reliably check the validity of NRQCD factorization and the universality of the LDMEs, one has to know the short-distance parts of the cross sections as precisely as possible. The hadroproduction of heavy quarkonia is presently being studied in a wide range of transverse momentum (p_T) and both at central and forward rapidities (y). To provide a uniform and accurate description of the short-distance parts of the cross sections is a challenging task even with state-of-the-art techniques in perturbative QCD.

Three characteristic p_T regions can be identified. In the region $p_T \lesssim M$, where M is the heavy-quarkonium mass, Sudakov-type double logarithms $\ln^2(p_T/M)$ spoil the convergence of the perturbative series in α_s and have to be resummed to reproduce the physical behavior of the cross section [4]. Moreover, small- x physics effects, such as the saturation of parton distribution functions (PDFs), can start to play a role there. In fact, at $\sqrt{S} = 7$ TeV, x values as small as 10^{-5} contribute to the lowest p_T bins for the rapidities covered by the LHCb detector [5]. At $p_T \gg M$, fragmentation logarithms $\ln(p_T/M)$ appear, and the description in terms of fragmentation functions, evolving with the energy scale, appears to be more appropriate [6]. In some intermediate p_T region, fixed-order calculations within the collinear parton model (CPM) should be valid. In the CPM, the complete next-to-leading-order (NLO) results for inclusive heavy-quarkonium production are available [7, 8]. The real-radiation part of the next-to-next-to-leading-order corrections to CS production was found to be sizable [9], even taking into account the large uncertainties due to the infrared cutoff scale.

The above-mentioned approaches appear to describe well the p_T distributions measured

in the respective regions. However, there is dramatic disagreement between the CO LDME sets extracted in different fits. Moreover, while a self-consistent description of all the experimental data of prompt J/ψ hadroproduction and photoproduction is possible at NLO in the CPM [7, 10], the LDMEs thus obtained lead to disagreement with the polarization measurements [11]. A similar, albeit less severe tension between the descriptions of yield and polarization was also observed for bottomonia [12]. This problem is usually referred to as the *heavy-quarkonium polarization puzzle*.

In view of the difficult situation described above, an approach which is equally appropriate on theoretical grounds both for the small- and large- p_T regions is required. Such an approach can be designed on the basis of the k_T factorization formalism [13] implemented with PDFs unintegrated over p_T (unPDFs), which naturally regularizes the small- p_T divergences that are present in fixed-order calculations within the CPM. The gauge independence of the hard-scattering matrix elements is, in general, broken by the virtuality of the initial-state gluons. To restore it, one can treat them as Reggeized gluons (Reggeons), which are the natural gauge-independent degrees of freedom of high-energy QCD. They were first introduced in the context of the Balitsky-Fadin-Kuraev-Lipatov (BFKL) [14] evolution equation and later promoted to the level of dynamical fields in Lipatov's effective action for the high-energy limit of QCD [15]. We denote the combination of the k_T factorization formalism for the cross sections with the Reggeization of partons in the initial state of the hard-scattering amplitudes as the parton Reggeization approach (PRA).

Presently, unPDFs are not so much constrained as collinear PDFs. However, there exists a method to obtain unPDFs from collinear ones, the Kimber-Martin-Ryskin (KMR) [16] model, which has produced stable and consistent results in many phenomenological applications. Besides numerous applications to charmonium [17–21] and bottomonium production [21–23], the PRA with KMR unPDFs has recently been successfully applied to describe the production of open charm [24], B mesons [25], dijets [26], bottom-flavored jets [27], Drell-Yan lepton pairs [28], monojets, and prompt photons [29] at the Fermilab Tevatron and the CERN LHC and to the associated production of photons and jets at DESY HERA [30].

In the present paper, we concentrate on the production of radially excited charmonium [$\psi(2S)$] and bottomonium [$\Upsilon(3S)$] states. This has the advantage that the feed-down contributions are negligibly small and so allows for direct tests of the underlying production mechanisms. The recent experimental data on the unpolarized $\psi(2S)$ yields from ATLAS

[31] and CMS [32] cover a wide p_T range and, in combination with CDF [33] and LHCb [34] data at smaller p_T values, allow us to quantitatively study the relative importance of the fusion and fragmentation production mechanisms. Measurements of J/ψ production from $\psi(2S)$ decay by CDF [35] and ATLAS [31] enable us to test a simple model of the feed-down kinematics [12, 36]. Furthermore, we exploit $\psi(2S)$ polarization data from CDF [37] and CMS [38] to address the question if the PRA can shed light on the notorious charmonium polarization puzzle. In the $\Upsilon(3S)$ case, we apply the PRA to interpret unpolarized-yield data by CDF [39], ATLAS [40], and LHCb [41] and polarization data by CDF [42] and CMS [43].

This paper is organized as follows. In Sec. II, we outline the basics of the PRA. Specifically, we describe both the fusion and fragmentation approximations at leading order (LO) in Sec. II A, and we list our analytic results for the polarization observables in Sec. II B. In Sec. III, we compare the selected experimental data with our numerical results. Specifically, Sec. III A is devoted to the unpolarized yields and Sec. III B to the polarization observables. In Sec. IV, we interpret the obtained results and summarize our conclusions.

II. BASIC FORMALISM

A. Unpolarized yields

The NRQCD factorization formalism [1] suggests that the effects of short and long distances are factorized in the partonic cross sections of the production of the heavy-quarkonium state \mathcal{H} as

$$d\hat{\sigma}^{\mathcal{H}} = \sum_n d\hat{\sigma}(Q\bar{Q}[n])\langle\mathcal{O}^{\mathcal{H}}[n]\rangle, \quad (1)$$

where the sum is over the possible intermediate Fock states $n = {}^{2S+1}L_J^{(a)}$ of the $Q\bar{Q}$ pair, with definite spin S , orbital momentum L , total angular momentum J , and CS or CO quantum numbers $a = 1, 8$, respectively. The decomposition in Eq. (1) corresponds to a double expansion in the strong-coupling constant α_s and the relative heavy-quark velocity v . The short-distance cross sections $d\hat{\sigma}(Q\bar{Q}[n])$ are perturbatively calculable, and the LDMEs $\langle\mathcal{O}^{\mathcal{H}}[n]\rangle$ possess definite v scaling properties [44]. For $\mathcal{H} = \psi(2S), \Upsilon(3S)$, the CS LDME $\langle\mathcal{O}^{\mathcal{H}}[{}^3S_1^{(1)}]\rangle$ contributes at $\mathcal{O}(v^3)$, and the CO LDMEs $\langle\mathcal{O}^{\mathcal{H}}[{}^1S_0^{(8)}]\rangle$, $\langle\mathcal{O}^{\mathcal{H}}[{}^3S_1^{(8)}]\rangle$, and $\langle\mathcal{O}^{\mathcal{H}}[{}^3P_J^{(8)}]\rangle$ ($J = 0, 1, 2$) contribute at $\mathcal{O}(v^7)$, while contributions of higher orders in v are

usually neglected.

The dominant contribution to inclusive heavy-quarkonium production at hadron colliders comes from the gluon fusion subprocess. In the PRA, its cross section can be represented as

$$d\sigma(pp \rightarrow \mathcal{H} + X) = \int \frac{dx_1}{x_1} \int \frac{d^2\mathbf{q}_{T1}}{\pi} \Phi_g(x_1, t_1, \mu_F^2) \int \frac{dx_2}{x_2} \int \frac{d^2\mathbf{q}_{T2}}{\pi} \Phi_g(x_2, t_2, \mu_F^2) d\hat{\sigma}^{\mathcal{H}}, \quad (2)$$

where the four-momenta q_i ($i = 1, 2$) of the Reggeons are parametrized as sums of longitudinal and transverse parts, $q_i = x_i P_i + q_{Ti}$, where P_i are the four-momenta of the colliding protons and $q_{Ti} = (0, \mathbf{q}_{Ti}, 0)$. We have $q_i^2 = -\mathbf{q}_{Ti}^2 = -t_i$ and $2P_1 \cdot P_2 = S$. In our approach, the gluon unPDF $\Phi_g(x, \mathbf{q}_T^2, \mu_F^2)$ is normalized relative to the collinear PDF by the following condition:

$$\int^{\mu_F^2} dt \Phi_g(x, t, \mu_F^2) = x f_g(x, \mu_F^2). \quad (3)$$

For the inelastic scattering of objects with hard intrinsic scales, such as photons with finite virtualities (Q^2), at high center-of-mass energies \sqrt{S} , the evolution of the unPDFs is governed by the large logarithms $\ln(S/Q^2)$ or $\ln(1/x)$ and is subject to the BFKL evolution equation [14]. In the production of particles with large p_T values, $\Lambda_{\text{QCD}} \ll p_T \ll \sqrt{S}$, in proton-proton collisions, the initial state does not provide a sufficiently hard intrinsic scale, so that the k_T -ordered Dokshitzer-Gribov-Lipatov-Altarelli-Parisi (DGLAP) [45] evolution at small values of k_T should be merged with the rapidity-ordered BFKL evolution at the final large- k_T steps of the initial-state-radiation cascade. The latter problem is highly nontrivial and equivalent to the complete resummation of the $\ln k_T$ -enhanced terms in the BFKL kernel. A few phenomenological schemes to compute unPDFs of the proton were proposed. In the present paper, we use the LO KMR unPDFs [16], generated from the LO set of Martin-Stirling-Thorne-Watt collinear PDFs [46]. Furthermore, we use the LO formula for α_s with normalization $\alpha_s(M_Z) = 0.12609$ and flavor thresholds at $m_c = 1.4$ GeV and $m_b = 4.75$ GeV.

We take into account the following $2 \rightarrow 1$ and $2 \rightarrow 2$ partonic subprocesses:

$$\begin{aligned} R(q_1) + R(q_2) &\rightarrow Q\bar{Q} \left[{}^1S_0^{(8)}, {}^3S_1^{(8)}, {}^3P_J^{(8)} \right], \\ R(q_1) + R(q_2) &\rightarrow Q\bar{Q} \left[{}^3S_1^{(1)} \right] + g, \end{aligned} \quad (4)$$

where R denotes the Reggeon. The matrix elements of the subprocesses in Eq. (4), summed over the polarizations of the final-state $Q\bar{Q}$ pair, were obtained in Ref. [18]. As shown in Ref. [18], our normalization conventions for the LDMEs coincide with those of Ref. [47].

In Ref. [20], CO LDMEs were fitted to Tevatron data of prompt J/ψ production in the following approximation. The charm-quark mass m_c was taken to be $m_c = M_{J/\psi}/2 \approx 1.5$ GeV, and the mass differences between the J/ψ meson and the excited χ_{cJ} and $\psi(2S)$ states were neglected in the respective feed-down contributions. This approximation is consistent with the NRQCD calculation at fixed order in v , since the mass difference ΔM is proportional to v^2 in the potential models. However, the kinematic effect of the mass splittings between charmonium states turns out to be significant. For the decay $\mathcal{H}_1 \rightarrow \mathcal{H}_2 + X$, the following approximate relation between the transverse momenta is valid in the limit $\Delta M \ll M_{\mathcal{H}_{1,2}}$:

$$\langle p_T^{\mathcal{H}_2} \rangle = \frac{M_{\mathcal{H}_2}}{M_{\mathcal{H}_1}} p_T^{\mathcal{H}_1} + \mathcal{O}\left(\frac{(\Delta M)^2}{M^2}, \frac{M}{p_T}\right), \quad (5)$$

where the averaging on the left-hand side is performed over the uniform distribution of the decay products in the rest frame of \mathcal{H}_1 . Due to the powerlike decrease of the p_T distribution at large p_T values, the small p_T shift in Eq. (5) can lead to a change in cross section by up to a factor of 2 in the case of charmonia and by up to 20%–30% in the case of bottomonia. In LO NRQCD calculations, the mass splitting can be taken into account only by appropriately adjusting the quark mass. In the present paper, we thus take $m_{c,b} = M_{\mathcal{H}}/2$. This approximation together with the shift in Eq. (5) was first adopted in Refs. [12, 36]. We would like to stress that the use of this kind of kinematic approximations actually violates the fixed-order character of the expansion in v implied by Eq. (1).

Since the LHC data cover values of p_T all the way up to 100 GeV, fragmentation corrections may be of vital importance for their description. In the LO-in- α_s plus leading-logarithmic (LL) approximation, only the $g \rightarrow Q\bar{Q}[{}^3S_1^{(8)}]$ transition acquires large logarithmic corrections of the type $\alpha_s \ln(p_T/M)$. In the large- p_T regime, the cross section of $pp \rightarrow \mathcal{H} + X$ may thus be approximately calculated as

$$\frac{d\sigma}{dp_T^{\mathcal{H}} dy_{\mathcal{H}}}(pp \rightarrow \mathcal{H} + X) = \int_0^1 dz \frac{d\sigma}{dp_T^g dy_g}(pp \rightarrow g) D_{g \rightarrow \mathcal{H}[{}^3S_1^{(8)}]}(z, \mu_F^2), \quad (6)$$

where $p_T^g = p_T^{\mathcal{H}}/z$ and $y_g = y_{\mathcal{H}}$. To LO in the PRA, we have

$$\frac{d\sigma}{dp_T^g dy_g}(pp \rightarrow g) = \frac{1}{(p_T^g)^3} \int_0^\infty dt_1 \int_0^{2\pi} d\phi_1 \Phi_g(x_1, t_1, \mu_F^2) \Phi_g(x_2, t_2, \mu_F^2) |\overline{\mathcal{M}(RR \rightarrow g)}|^2, \quad (7)$$

where $|\overline{\mathcal{M}(RR \rightarrow g)}|^2 = (3/2)\pi\alpha_s(\mu_R^2)(p_T^g)^2$ is the squared amplitude obtained from the Fadin-Lipatov effective Reggeon-Reggeon-gluon vertex [14, 29] and $t_2 = t_1 + (p_T^g)^2 -$

$2p_T^g \sqrt{t_1} \cos \phi_1$. The fragmentation function $D_{g \rightarrow \mathcal{H}[{}^3S_1^{(8)}]}(z, \mu_F^2)$ is obtained by solving the LO DGLAP evolution equation [45] with the initial condition

$$D_{g \rightarrow \mathcal{H}[{}^3S_1^{(8)}]}(z, \mu_{F0}^2) = \frac{\pi \alpha_s(\mu_{F0}^2)}{6M_{\mathcal{H}}^3} \left\langle \mathcal{O}^{\mathcal{H}} [{}^3S_1^{(8)}] \right\rangle \delta(1-z), \quad (8)$$

at the starting scale $\mu_{F0}^2 = M_{\mathcal{H}}^2$. The explicit form of the solution can be found, *e.g.*, in Ref. [17]. In the following, we shall refer to the production mechanism underlying Eqs. (6)–(8) as fragmentation and the one underlying the usual treatment of the ${}^3S_1^{(8)}$ contribution [18–23] as fusion.

We take the renormalization and factorization scales to be $\mu_F = \mu_R = \xi M_T$, where $M_T = \sqrt{M_{\mathcal{H}}^2 + p_T^2}$ is the transverse mass, and vary ξ by a factor of 2 up and down about the default value 1 to estimate the scale uncertainty.

B. Polarization parameters

The polarization parameters λ_θ , λ_φ , and $\lambda_{\theta\varphi}$ are defined through the angular distribution of the leptonic decay $\mathcal{H} \rightarrow l^+ l^-$ in the rest frame of the 3S_1 heavy-quarkonium state \mathcal{H} ,

$$\frac{d\sigma}{d\Omega} \propto 1 + \lambda_\theta \cos^2 \theta + \lambda_\varphi \sin^2 \theta \cos(2\varphi) + \lambda_{\theta\varphi} \sin(2\theta) \cos \varphi, \quad (9)$$

where θ and φ are the polar and azimuthal angles of the flight direction of lepton l^+ in some appropriately chosen coordinate system. This choice is an important issue, which is widely discussed in the literature, see, *e.g.*, Refs. [48, 49]. In the present study, we concentrate on the polarization parameter λ_θ in the s -channel helicity frame, where the longitudinal polarization vector points along the z axes and can be written in covariant form as

$$\varepsilon^\mu(0) = Z^\mu = \frac{(p \cdot Q)p^\mu / M - M Q^\mu}{\sqrt{(p \cdot Q)^2 - M^2 S}}, \quad (10)$$

with p being the four-momentum of \mathcal{H} and $Q = P_1 + P_2$. The calculation of λ_θ in the PRA proceeds along the same lines as in the CPM [48, 50, 51], and we merely list our results. We have

$$\lambda_\theta = \frac{\sigma^{\mathcal{H}} - 3\sigma_L^{\mathcal{H}}}{\sigma^{\mathcal{H}} + \sigma_L^{\mathcal{H}}}, \quad (11)$$

where $\sigma_L^{\mathcal{H}}$ is the cross section for the production of the heavy-quarkonium state \mathcal{H} with longitudinal polarization, $J_z = 0$, and $\sigma^{\mathcal{H}}$ is summed over $J_z = 0, \pm 1$ as in Sec. II A. Assuming the polarizations of the ${}^3S_1^{(1)}$ and ${}^3S_1^{(8)}$ states to be directly transferred to the \mathcal{H}

meson and chromoelectric-dipole transitions with $\Delta S = 0$ and $\Delta L = 1$ from the 3P_J states [52], we have

$$\begin{aligned} \sigma_L^{\mathcal{H}} = & \sigma_0^{\mathcal{H}} \left[{}^3S_1^{(1)} \right] + \sigma_0^{\mathcal{H}} \left[{}^3S_1^{(8)} \right] + \frac{1}{3} \left(\sigma^{\mathcal{H}} \left[{}^1S_0^{(8)} \right] + \sigma^{\mathcal{H}} \left[{}^3P_0^{(8)} \right] \right) + \frac{1}{2} \left(\sigma_1^{\mathcal{H}} \left[{}^3P_1^{(8)} \right] + \sigma_1^{\mathcal{H}} \left[{}^3P_2^{(8)} \right] \right) \\ & + \frac{2}{3} \sigma_0^{\mathcal{H}} \left[{}^3P_2^{(8)} \right], \end{aligned} \quad (12)$$

where the label J_z in the notation $\sigma_{|J_z|}^{\mathcal{H}}[n]$ refers to the $Q\bar{Q}$ Fock state n rather than the heavy-quarkonium state \mathcal{H} . The relevant matrix element squares $|\overline{\mathcal{M}_{|J_z|}(RR \rightarrow \mathcal{H}[n])}|^2$ for fixed value of $|J_z|$, averaged over the spins and colors of the incoming Reggeons, are given by

$$\begin{aligned} \left| \overline{\mathcal{M}_0(RR \rightarrow \mathcal{H} [{}^3S_1^{(8)}])} \right|^2 &= 2\pi^2 \alpha_s^2 \frac{\langle \mathcal{O}^{\mathcal{H}} [{}^3S_1^{(8)}] \rangle}{M^3} \\ &\quad \times \frac{M^2 M_T^2 (t_1 x_1 - t_2 x_2)^2 \cos^2 \varphi}{(M^2 + t_1 + t_2)^2 [M^2 (x_1 - x_2)^2 + p_T^2 (x_1 + x_2)^2]}, \\ \left| \overline{\mathcal{M}_0(RR \rightarrow \mathcal{H} [{}^3P_1^{(8)}])} \right|^2 &= \left| \overline{\mathcal{M}(RR \rightarrow \mathcal{H} [{}^3P_1^{(8)}])} \right|^2 - \left| \overline{\mathcal{M}_1(RR \rightarrow \mathcal{H} [{}^3P_1^{(8)}])} \right|^2 \\ &= \frac{20}{9} \pi^2 \alpha_s^2 \frac{\langle \mathcal{O}^{\mathcal{H}} [{}^3P_1^{(8)}] \rangle}{M^5} \\ &\quad \times \frac{M^2 M_T^6 (t_1 + t_2)^2 (x_1 + x_2)^2 \sin^2 \varphi}{(M^2 + t_1 + t_2)^4 [M^2 (x_1 - x_2)^2 + p_T^2 (x_1 + x_2)^2]}, \\ \left| \overline{\mathcal{M}_0(RR \rightarrow \mathcal{H} [{}^3P_2^{(8)}])} \right|^2 &= \frac{4}{9} \pi^2 \alpha_s^2 \frac{\langle \mathcal{O}^{\mathcal{H}} [{}^3P_2^{(8)}] \rangle}{M^5} \\ &\quad \times \frac{M^2 M_T^4 [M_T^2 (x_1 + x_2)^2 + 2M^2 x_1 x_2]^2}{(M^2 + t_1 + t_2)^4 [M^2 (x_1 - x_2)^2 + p_T^2 (x_1 + x_2)^2]^2} \\ &\quad \times [(t_1 + t_2) \cos \varphi + 2\sqrt{t_1 t_2}]^2, \\ \left| \overline{\mathcal{M}_1(RR \rightarrow \mathcal{H} [{}^3P_2^{(8)}])} \right|^2 &= \frac{4}{3} \pi^2 \alpha_s^2 \frac{\langle \mathcal{O}^{\mathcal{H}} [{}^3P_2^{(8)}] \rangle}{M^5} \\ &\quad \times \frac{M^4 M_T^6 (x_1 + x_2)^2}{(M^2 + t_1 + t_2)^4 [M^2 (x_1 - x_2)^2 + p_T^2 (x_1 + x_2)^2]^2} \\ &\quad \times \left\{ p_T^2 [M_T^2 (x_1^2 + x_2^2) - 2M^2 x_1 x_2] - 2x_1 x_2 [(t_1^2 + t_2^2) \cos(2\varphi) \right. \\ &\quad \left. + 4(t_1 + t_2) \sqrt{t_1 t_2} \cos \varphi + 6t_1 t_2] \right\}, \end{aligned} \quad (13)$$

where φ is the angle enclosed between \mathbf{q}_{T1} and \mathbf{q}_{T2} . Our result for a longitudinally polarized ${}^3S_1^{(1)}$ state is too lengthy to be present here.

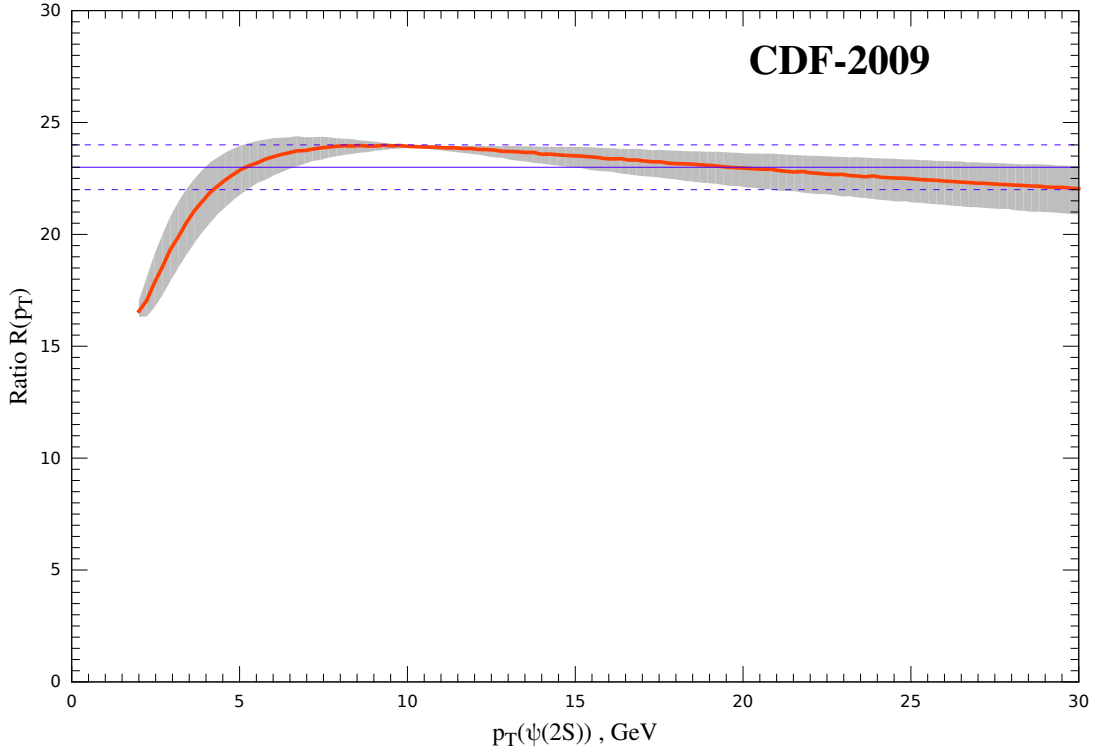


FIG. 1: Ratio $R_{\psi(2S)}$ defined in Eq. (14) as a function on p_T under CDF-2009 [33] kinematic conditions (thick solid orange line) and its theoretical uncertainty (shaded band). The average value $R_{\psi(2S)} = 23.0 \pm 1.0$ (thin solid and dashed blue lines) is shown for comparison.

III. NUMERICAL RESULTS

A. Unpolarized yields

We are now in a position to compare the p_T distributions of unpolarized $\psi(2S)$ and $\Upsilon(3S)$ mesons measured at the Tevatron and the LHC with our theoretical predictions. The values of the CS LDMEs $\langle \mathcal{O}^{\psi(2S)} [3S_1^{(1)}] \rangle$ and $\langle \mathcal{O}^{\Upsilon(3S)} [3S_1^{(1)}] \rangle$ listed in Table I are adopted from Refs. [3, 50], where they were determined from the total width of the $\psi(2S) \rightarrow \mu^+ \mu^-$ decay and a potential model, respectively.

We start with the $\psi(2S)$ case. The CDF Collaboration measured the p_T distribution of prompt $\psi(2S)$ mesons at $\sqrt{S} = 1.96$ TeV for pseudorapidities $|\eta| < 0.6$ in the range $2 \text{ GeV} < p_T < 30 \text{ GeV}$ by reconstructing their $\psi(2S) \rightarrow \mu^+ \mu^-$ decays (CDF-2009) [33]. Here and in the following, $p_T \equiv p_T^{\psi(2S)}$, $y \equiv y_{\psi(2S)}$, and $\eta \equiv \eta_{\psi(2S)}$. For such moderate p_T values, the fusion approximation is expected to be appropriate. At LO and NLO in the

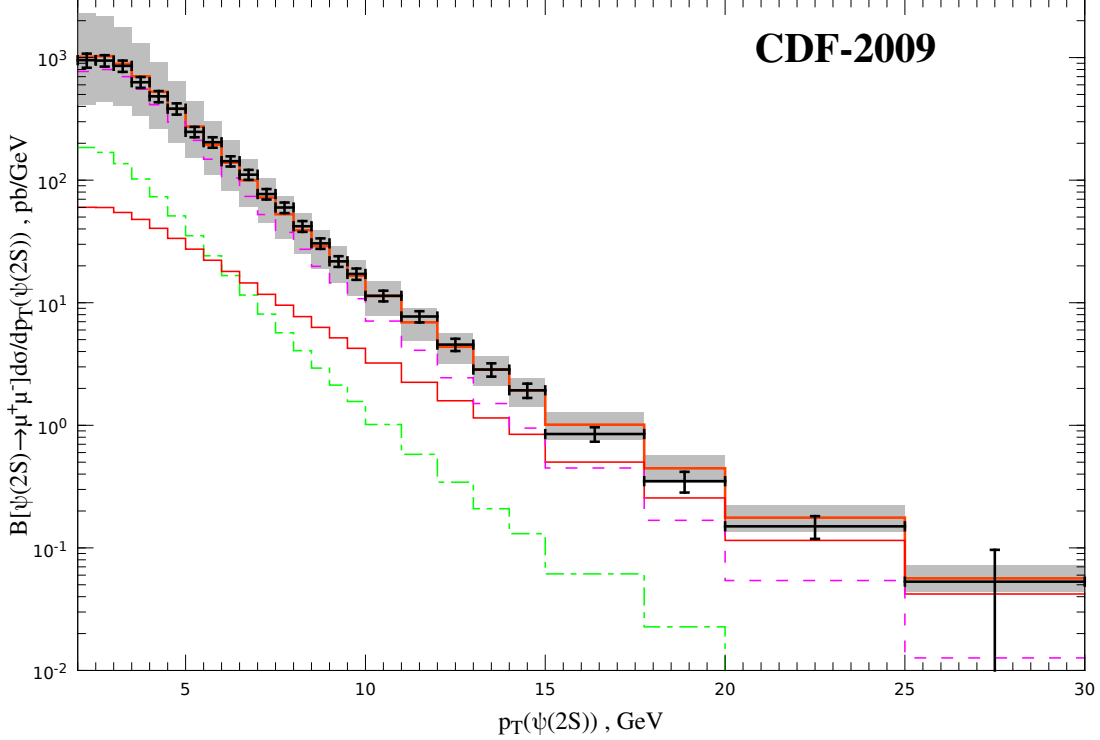


FIG. 2: The CDF-2009 [33] data set on the p_T distribution of $\psi(2S)$ inclusive hadroproduction is compared with the fitted LO PRA result in the fusion approximation (thick solid orange histogram) and its theoretical uncertainty (shaded band). The ${}^3S_1^{(1)}$ (thin dot-dashed green histogram), ${}^3S_1^{(8)}$ (thin solid red histogram), and mixed ${}^1S_0^{(8)}$ and ${}^3P_J^{(8)}$ (thin dashed violet histogram) contributions are shown for comparison.

CPM, fits of the J/ψ and $\psi(2S)$ CO LDMEs to hadroproduction data are known to fail to separately determine $\langle \mathcal{O}^{\mathcal{H}} [{}^1S_0^{(8)}] \rangle$ and $\langle \mathcal{O}^{\mathcal{H}} [{}^3P_J^{(8)}] \rangle$ because the respective p_T distributions exhibit very similar line shapes [7, 36]. In Fig. 1, we investigate if this problem carries over to the PRA by considering the ratio

$$R_{\mathcal{H}}(p_T) = \frac{M_{\mathcal{H}}^2 \sum_{J=0}^2 (2J+1) d\sigma/dp_T [{}^3P_J^{(8)}]}{d\sigma/dp_T [{}^1S_0^{(8)}]}, \quad (14)$$

for $\mathcal{H} = \psi(2S)$ together with its scale uncertainty as a function of p_T under CDF-2009 kinematic conditions. We observe that the fraction $R_{\psi(2S)}(p_T)$ varies very feebly in the interval $5 \text{ GeV} < p_T < 30 \text{ GeV}$ and can be well approximated by the constant $R_{\psi(2S)} = 23.0 \pm 1.0$, while its numerator and denominator themselves vary by several orders of magnitude. In

view of the considerable experimental errors and the scale uncertainties of the theoretical predictions, it is thus unfeasible to separately determine $\langle \mathcal{O}^{\psi(2S)} [^1S_0^{(8)}] \rangle$ and $\langle \mathcal{O}^{\psi(2S)} [^3P_0^{(8)}] \rangle$ by just fitting large- p_T data. Instead, we introduce the linear combination

$$M_R^{\mathcal{H}} = \langle \mathcal{O}^{\mathcal{H}} [^1S_0^{(8)}] \rangle + \frac{R_{\mathcal{H}}}{M_{\mathcal{H}}^2} \langle \mathcal{O}^{\mathcal{H}} [^3P_0^{(8)}] \rangle \quad (15)$$

for $\mathcal{H} = \psi(2S)$. Our fit to the CDF-2009 [33] data is excellent, as is evident from Fig. 2, yielding just $\chi^2/\text{d.o.f.} = 0.6$. The resulting fit parameters are listed in Table I.

Here and in the following, the theoretical-error bands are evaluated by combining the scale variations and the LDME errors in quadrature. The latter include the simultaneous variations of $\langle \mathcal{O}^{\mathcal{H}} [^1S_0^{(8)}] \rangle$ and $\langle \mathcal{O}^{\mathcal{H}} [^3P_0^{(8)}] \rangle$ in compliance with their positivity and Eq. (15). The LO KMR unPDFs [16] adopted here are uniquely fixed by the underlying collinear PDFs [46], and we neglect this source of theoretical uncertainty. Given the present theoretical uncertainties in the CO LDMEs, the hadroproduction of heavy quarkonia does not yet provide a useful laboratory to constrain the proton unPDFs. Precision data of the proton structure functions in deeply inelastic scattering [55] or of the associated hadroproduction of electroweak gauge bosons and jets [56] are much more powerful in this respect.

In the PRA, the divergent behavior of the p_T distribution at small p_T values is regularized by the Sudakov form factor in the KMR [16] unPDF, which opens the possibility to include small- p_T data in the fit. However, as is clear from Figs. 1 and 2, our present LO-plus-LL analysis has the largest scale uncertainty in the small- p_T region, reaching a factor of 2 in the first p_T bin. Under the influence of the small- p_T data, our fit slightly prefers the $^3P_J^{(8)}$ contribution, which is actually included in Fig. 2, over the $^1S_0^{(8)}$ one. However, this finding should not be taken too seriously.

The CDF Collaboration also measured the $p_T^{J/\psi}$ distribution of J/ψ mesons from $\psi(2S) \rightarrow J/\psi + X$ decays at $\sqrt{S} = 1.8$ TeV for $|\eta_{J/\psi}| < 0.6$ in the range $5 \text{ GeV} < p_T^{J/\psi} < 20 \text{ GeV}$ (CDF-1997) [35]. In Fig. 3, we compare these data with our LO PRA prediction evaluated in the fusion approximation using the LDMEs determined above and with the p_T shift introduced in Eq. (5). We find excellent agreement within the experimental and theoretical uncertainties, which nicely confirms the kinematic approximation underlying Eq. (5).

The ATLAS Collaboration presented their sample of $\psi(2S) \rightarrow J/\psi + \pi^+\pi^-$ decays collected at $\sqrt{S} = 7$ TeV as distributions in p_T and $p_T^{J/\psi}$ in the range $10 \text{ GeV} < p_T, p_T^{J/\psi} < 100 \text{ GeV}$ for three bins in $|y|$ and $|y_{J/\psi}|$, respectively (ATLAS-2014) [31]. The CMS Collab-

LDME	Fusion	Fragmentation	NLO CPM [12, 36]	NLO CPM [54]
$\langle \mathcal{O}^{\psi(2S)} [{}^3S_1^{(1)}] \rangle / \text{GeV}^3$	0.65 ± 0.06 [50]	0.65 ± 0.06 [50]	0.76 [3]	0.76 [3]
$\langle \mathcal{O}^{\psi(2S)} [{}^3S_1^{(8)}] \rangle / \text{GeV}^3 \times 10^3$	1.84 ± 0.23	2.57 ± 0.09	1.2 ± 0.3	2.80 ± 0.49
$M_R^{\psi(2S)} / \text{GeV}^3 \times 10^2$	3.11 ± 0.14	2.70 ± 0.11	2.0 ± 0.6	0.37 ± 4.85
$R_{\psi(2S)}$	23.0 ± 1.0	23.0 ± 1.0	23.5	23.0
$\chi^2/\text{d.o.f.}$	0.6	1.1	0.56	2.84
$\langle \mathcal{O}^{\Upsilon(3S)} [{}^3S_1^{(1)}] \rangle / \text{GeV}^3$	3.54 [3]	\dots	3.54 [3]	\dots
$\langle \mathcal{O}^{\Upsilon(3S)} [{}^3S_1^{(8)}] \rangle / \text{GeV}^3 \times 10^2$	2.73 ± 0.15	\dots	2.71 ± 0.13	\dots
$M_R^{\Upsilon(3S)} / \text{GeV}^3 \times 10^2$	0.00 ± 0.18	\dots	1.08 ± 1.66	\dots
$R_{\Upsilon(3S)}$	22.1 ± 0.7	\dots	22.1	\dots
$\chi^2/\text{d.o.f.}$	9.7	\dots	3.16	\dots

TABLE I: $\psi(2S)$ and $\Upsilon(3S)$ LDME sets. The CS LDMEs [3, 50] are input. The $\psi(2S)$ CO LDMEs are fitted to the CDF-2009 [33] data in the fusion approximation and to the ATLAS-2014 [31] and the CMS-2015 [32] data in the fragmentation approximation. The $\Upsilon(3S)$ CO LDMEs are fitted to the ATLAS-2013 [40] data in the fusion approximation. $M_R^{\mathcal{H}}$ and $R_{\mathcal{H}}$ are defined in Eq. (15). The errors in the CO LDMEs are multiplied by $\sqrt{\chi^2/\text{d.o.f.}}$ if $\chi^2/\text{d.o.f.} > 1$ as it is done, *e.g.*, in Ref. [53]. The results of the NLO CPM fits for the $\psi(2S)$ meson in Refs. [36, 54] and for the $\Upsilon(3S)$ meson in Ref. [12] are listed for comparison.

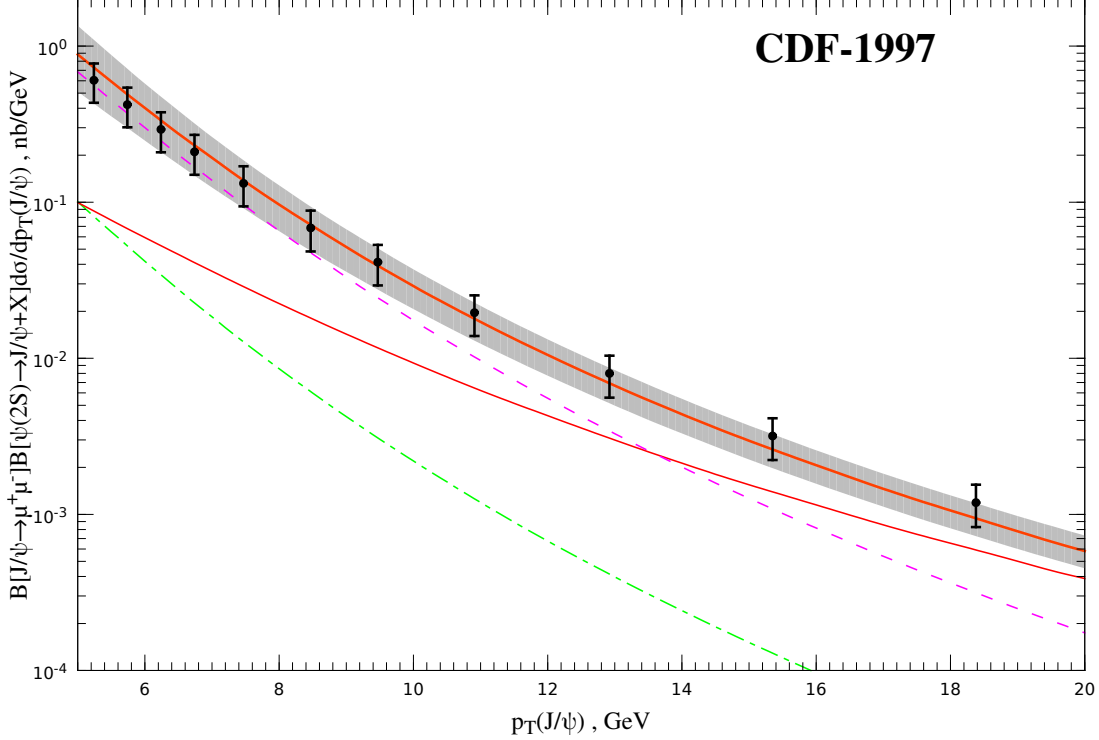


FIG. 3: The CDF-1997 [35] data set on the $p_T^{J/\psi}$ distribution of J/ψ mesons from $\psi(2S)$ decay is compared with the predicted LO PRA result in the fusion approximation evaluated using Eq. (5) (thick solid orange line) and its theoretical uncertainty (shaded band). The ${}^3S_1^{(1)}$ (thin dot-dashed green line), ${}^3S_1^{(8)}$ (thin solid red line), and mixed ${}^1S_0^{(8)}$ and ${}^3P_J^{(8)}$ (thin dashed violet line) contributions are shown for comparison.

oration measured the p_T distribution of $\psi(2S)$ mesons at $\sqrt{S} = 7$ TeV for 4 bins in $|y|$ in the range $10 \text{ GeV} < p_T < 75 \text{ GeV}$ by reconstructing their $\psi(2S) \rightarrow \mu^+ \mu^-$ decays (CMS-2015) [32]. The ATLAS-2014 and CMS-2015 data may be well described in the fusion approximation with the corresponding LDME set determined above in the lower p_T range, below 30 GeV say. On the other hand, this approximation badly fails for the largest p_T values probed by these data. Since the fragmentation approximation as introduced in Sec. II only affects the ${}^3S_1^{(8)}$ contribution, which is suppressed for small values of p_T , as may be seen from Figs. 2 and 3, it should be appropriate for the ATLAS-2014 and CMS-2015 data, which set on at $p_T = 10$ GeV. In fact, our joint LO PRA fit in the fragmentation approximation to the double-differential cross sections $d^2\sigma/(dp_T dy)$ measured by ATLAS [31] and CMS [32] yield an excellent description of these data, with $\chi^2/\text{d.o.f.} = 1.1$, which is reflected by Figs. 4 and

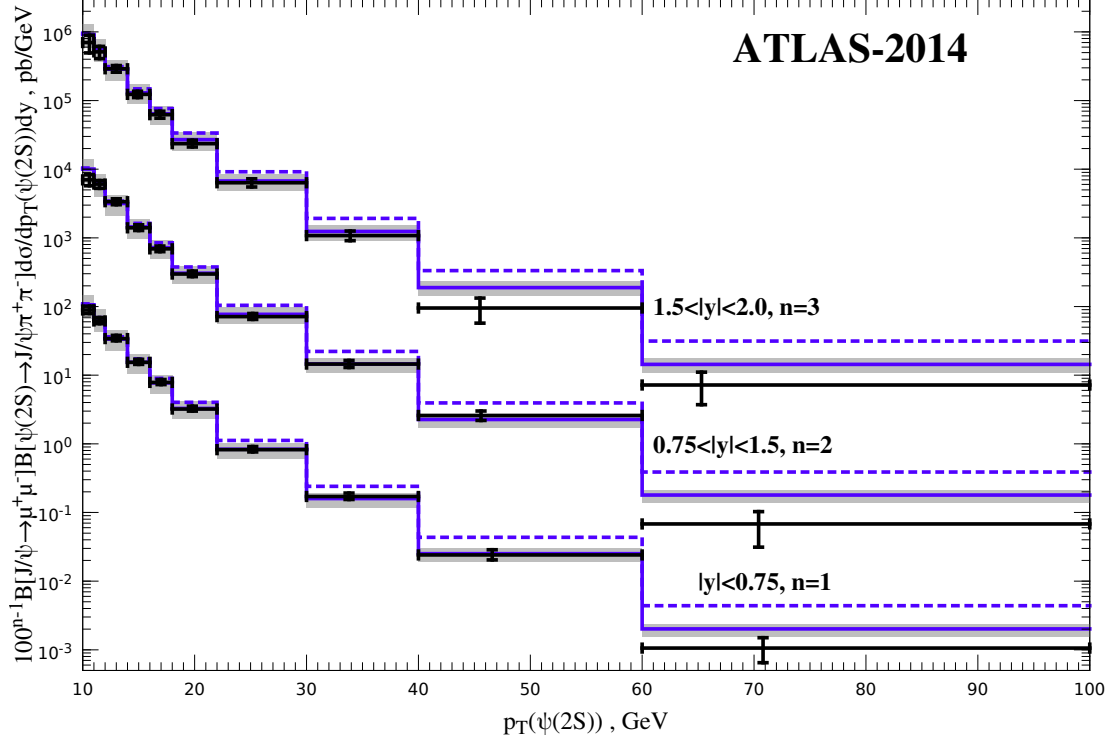


FIG. 4: The ATLAS-2014 [31] data sets on the p_T distributions of $\psi(2S)$ inclusive hadroproduction, multiplied by 100 for $0.75 < |y| < 1.5$ and by 10 000 for $1.5 < |y| < 2.0$ for better visibility, are compared with the fitted LO PRA results in the fragmentation approximation (thick solid blue histograms) and their theoretical uncertainties (shaded bands). The LO PRA results in the fusion approximation (thick dashed blue histograms) are shown for comparison.

5, respectively. The fit results are listed in Table I; they are in the same ball park as those extracted from the CDF-2009 data in the fusion approximation.

For comparison, we quote in Table I also the values of the LDMEs recently obtained through NLO CPM fits in Refs. [12, 36, 54].¹ A comparison with NLO CPM results is justified because the LO PRA approximation captures important classes of corrections that lie beyond the LO CPM treatment. The lack of discriminating power of the hadroproduction yield was also experienced in Refs. [12, 36]. By contrast, the fit in Ref. [54] included orthogonal information from photoproduction and could so separately fix the values of $\langle \mathcal{O}^{\psi(2S)} [1S_0^{(8)}] \rangle$ and $\langle \mathcal{O}^{\psi(2S)} [3P_0^{(8)}] \rangle$, which are combined assuming $R_{\psi(2S)} = 23.0$ as in

¹ The fit results of Ref. [54] were used for theoretical predictions included in Ref. [57].

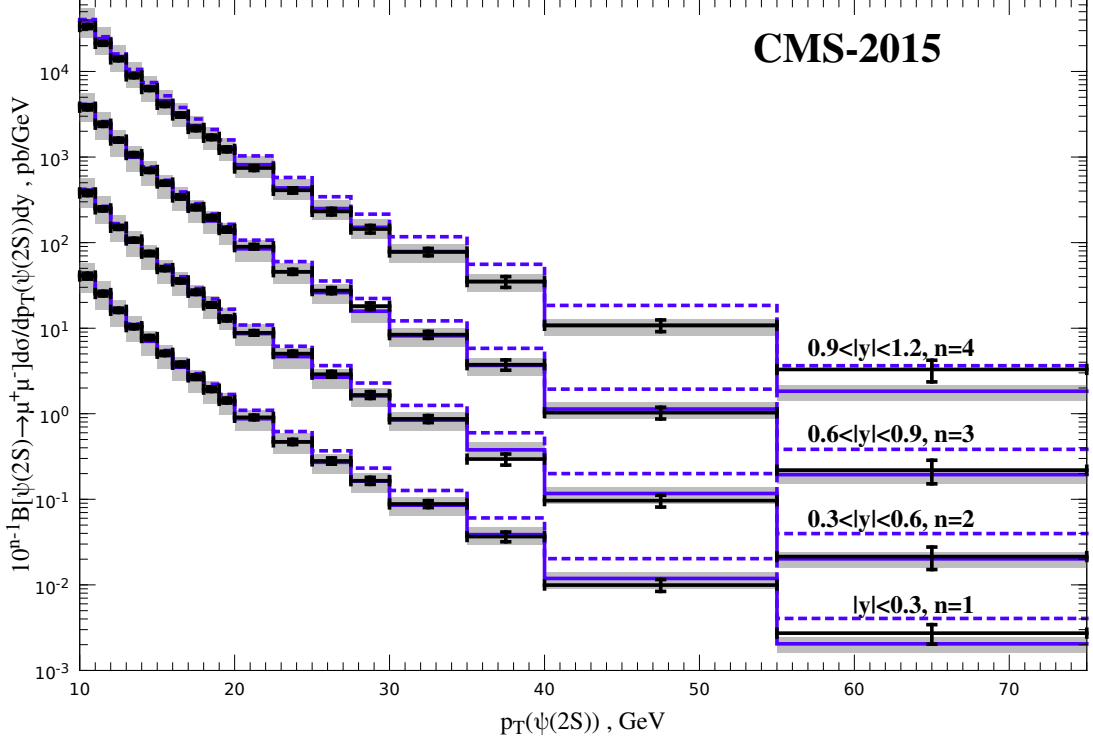


FIG. 5: The CMS-2015 [32] data sets on the p_T distributions of $\psi(2S)$ inclusive hadroproduction, multiplied by 10 for $0.3 < |y| < 0.6$, by 100 for $0.6 < |y| < 0.9$, and by 1000 for $0.9 < |y| < 1.2$ for better visibility, are compared with the fitted LO PRA results in the fragmentation approximation (thick solid blue histograms) and their theoretical uncertainties (shaded bands). The LO PRA results in the fusion approximation (thick dashed blue histograms) are shown for comparison.

our LO PRA fit in the fusion approximation to give the value of $M_R^{\psi(2S)}$ specified in Table I. The small difference between the values of $\langle \mathcal{O}^{\psi(2S)} [{}^3S_1^{(1)}] \rangle$ extracted in Refs. [3, 50] is irrelevant for this comparison because the ${}^3S_1^{(1)}$ contribution is greatly suppressed. We observe from Table I that the NLO CPM fit results [12, 36, 54] are comparable with the LO PRA ones.

Figures 4 and 5 also contain the LO PRA predictions evaluated in the fusion approximation using the respective LDME set from Table I. As anticipated above, these predictions usefully describe the ATLAS-2014 and CMS-2015 data for $p_T \lesssim 30$ GeV. On the other hand, they greatly overshoot the data and their LO PRA description in the fragmentation approximation at large p_T values. We conclude that the fusion and fragmentation approximations are consistent in the lower p_T range, and that the fragmentation corrections are

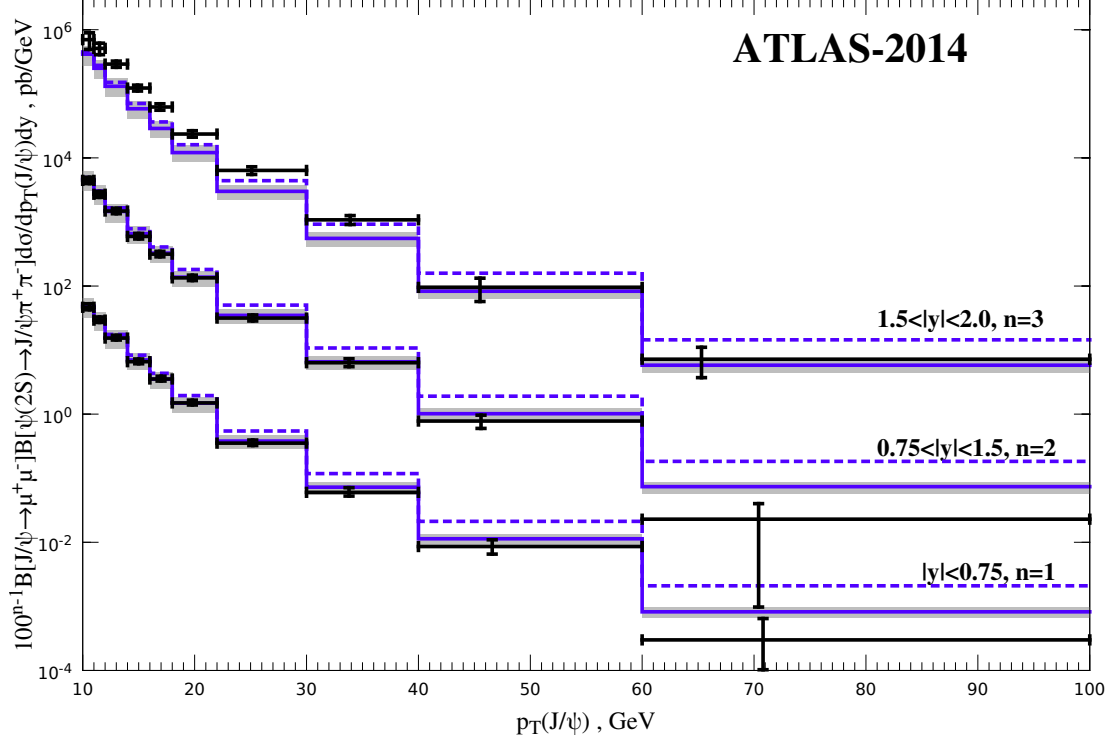


FIG. 6: The ATLAS-2014 [31] data sets on the $p_T^{J/\psi}$ distributions of J/ψ mesons from $\psi(2S)$ decay, multiplied by 100 for $0.75 < |y_{J/\psi}| < 1.5$ and by 10 000 for $1.5 < |y_{J/\psi}| < 2.0$ for better visibility, are compared with the predicted LO PRA results in the fragmentation approximation evaluated using Eq. (5) (thick solid blue histograms) and their theoretical uncertainties (shaded bands). The LO PRA results in the fusion approximation (thick dashed blue histograms) are shown for comparison.

very important in the upper p_T range.

In Fig. 6, we compare the $p_T^{J/\psi}$ distributions of the J/ψ mesons from $\psi(2S)$ decays measured by ATLAS [31] in the three $|y_{J/\psi}|$ bins with our LO PRA predictions evaluated in the fragmentation approximation with the corresponding LDMEs in Table I and the p_T shift in Eq. (5). For comparison, we also present the corresponding results in the fusion approximation. Except for the most forward $|y_{J/\psi}|$ bin, we encounter a similar qualitative picture as in Fig. 4 for the p_T distribution of the ATLAS-2014 data, which is typically a factor of 2 larger. In fact, the fragmentation approximation nicely describes the data in the entire $p_T^{J/\psi}$ range and is consistent with the fusion approximation in the lower $p_T^{J/\psi}$ range. As in the case of the CDF-1997 data in Fig. 3, the kinematic approximation in Eq. (5) proves

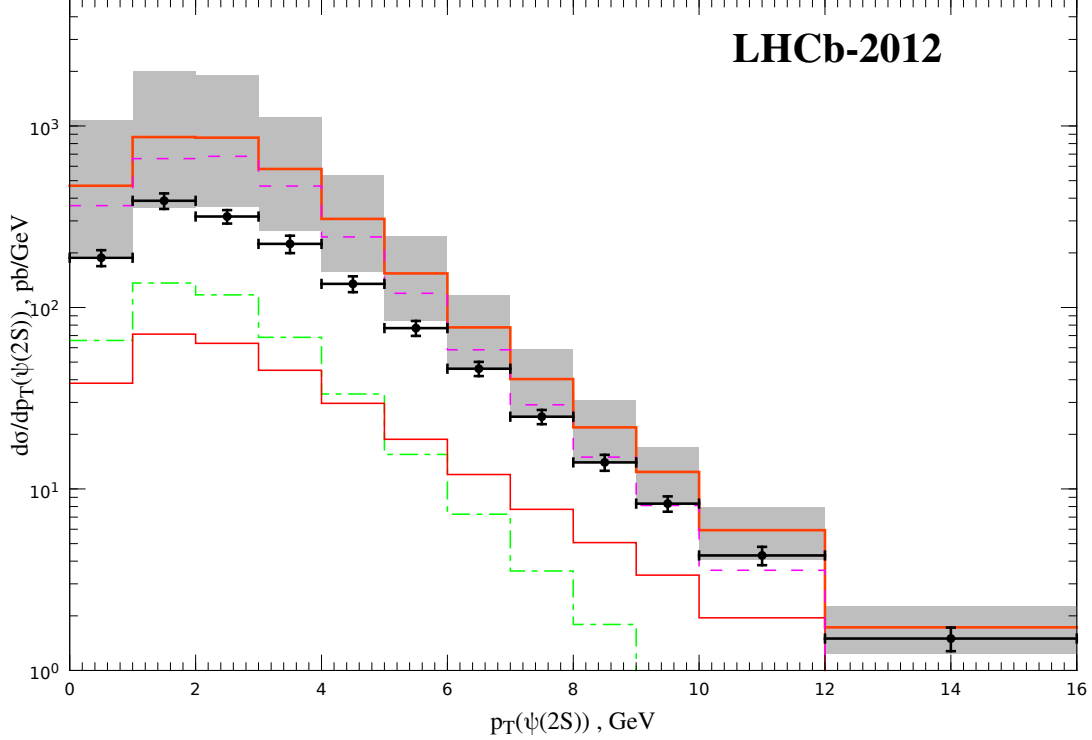


FIG. 7: The LHCb-2012 [34] data set on the p_T distribution of $\psi(2S)$ inclusive hadroproduction is compared with the predicted LO PRA result in the fusion approximation (thick solid orange histogram) and its theoretical uncertainty (shaded band). The ${}^3S_1^{(1)}$ (thin dot-dashed green histogram), ${}^3S_1^{(8)}$ (thin solid red histogram), and mixed ${}^1S_0^{(8)}$ and ${}^3P_J^{(8)}$ (thin dashed violet histogram) contributions are shown for comparison.

to be sufficiently accurate at the LO PRA level, at least for central $y_{J/\psi}$ values.

The above comparisons were performed for measurements at central rapidities. This kinematic region is most suitable for the application of the PRA, since most of the initial-state radiation can be considered as highly separated in rapidity. The LHCb Collaboration measured the $\psi(2S)$ p_T distribution for $p_T < 16$ GeV at $\sqrt{S} = 7$ TeV in the forward region $2.0 < y < 4.5$ (LHCb-2012) [34]. In Fig. 7, we compare this measurement with our LO PRA predictions in the fusion approximation. We find that the LHCb-2012 data mostly lie at the lower edge of the theoretical error band. We hence conclude that the LO PRA approximation with both initial-state gluons being Reggeized is less appropriate for this kinematic region.

We now turn to the unpolarized $\Upsilon(3S)$ yield. The ATLAS Collaboration measured the

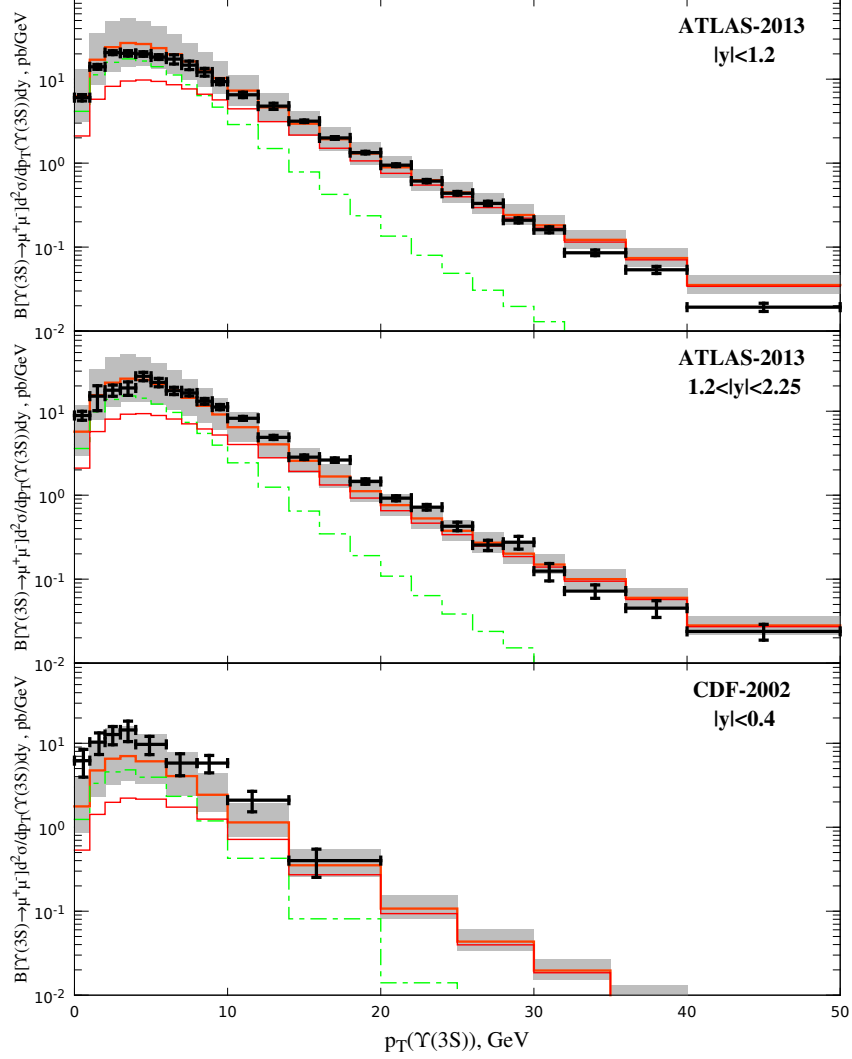


FIG. 8: The ATLAS-2013 [40] (upmost and center panels) and CDF-2002 [39] (downmost panel) data sets on the p_T distributions of $\Upsilon(3S)$ inclusive hadroproduction are compared with the fitted and predicted LO PRA results in the fusion approximation (thick solid orange histograms) and their theoretical uncertainties (shaded bands), respectively. The ${}^3S_1^{(1)}$ (thin dot-dashed green histograms) and ${}^3S_1^{(8)}$ (thin solid red histograms) contributions are shown for comparison. The mixed ${}^1S_0^{(8)}$ and ${}^3P_J^{(8)}$ contribution does not contribute due to $M_R^{\Upsilon(3S)} = 0$ in Table I.

p_T distribution of $\Upsilon(3S)$ mesons at $\sqrt{S} = 7$ TeV in two different $|y|$ bins in the range $p_T < 50$ GeV by reconstructing their $\Upsilon(3S) \rightarrow \mu^+\mu^-$ decays (ATLAS-2013) [40]. In view of $m_{\Upsilon(3S)} = 10.123$ GeV, the fusion approximation is certainly appropriate here. Our LO PRA fit to the ATLAS-2013 data in the bins $|y| < 1.2$ and $1.2 < |y| < 2.5$ yields $\chi^2/\text{d.o.f.} = 9.7$

and is presented in the upmost and center panels of Fig. 8, respectively. The hierarchy of the various contributions in the $\Upsilon(3S)$ case is completely different from the $\psi(2S)$ case. While the ${}^3S_1^{(1)}$ contribution is almost negligible in the $\psi(2S)$ case, it dominates for small p_T values in the $\Upsilon(3S)$ case, leaving little room for the ${}^1S_0^{(8)}$ and ${}^3P_J^{(8)}$ contributions.

The fit values of the CO LDMEs are listed in Table I; the ratio $R_{\Upsilon(3S)}(p_T)$ defined in Eq. (14) is again approximately constant, namely $R_{\Upsilon(3S)} = 22.1 \pm 0.7$. The analogous values in Ref. [23] are slightly different because they were obtained using $m_b = M_{\Upsilon(1S)}/2$ rather than $m_b = M_{\Upsilon(3S)}/2$, the choice used here. For comparison, the values of the $\Upsilon(3S)$ CO LDMEs extracted in Ref. [12] are also quoted in Table I. They are compatible with our results.

$\Upsilon(3S)$ p_T distributions were also measured by the CDF Collaboration at $\sqrt{S} = 1.8$ GeV for $|y| < 0.4$ (CDF-2002) [39] and by the LHCb Collaboration at $\sqrt{S} = 7$ GeV in five y bins (LHCb-2012a) [41]. These data are confronted with our LO PRA predictions in the downmost panel of Fig. 8 and in Figs. 9 and 10, respectively. The CDF-2002 data tend lie at the upper edge of our theoretical error band, while the LHCb-2012a data exhibit nice agreement, with a few exceptions, which appear to be runaway data points. At this point, the question naturally arises why LO PRA works at large y values for $\Upsilon(3S)$ in Figs. 9 and 10, while it fails for $\psi(2S)$ in Fig. 3. A possible explanation for this may be related to the fact that the $\Upsilon(3S)$ yield is dominated by the ${}^3S_1^{(1)}$ contribution at small p_T values, while the $\psi(2S)$ yield is almost exhausted by the ${}^1S_0^{(8)}$ and ${}^3P_J^{(8)}$ contributions. In fact, the CO states could be partly destroyed by soft- or Glauber-gluon exchanges with other partons populating the forward region, while the CS state survives. We, therefore, propose a more detailed study of the y dependencies of the $\psi(2S)$ and $\Upsilon(3S)$ production cross sections as a promising test of the k_T -factorization-breaking effects.

In Ref. [58], the CMS Collaboration compare their measurements of the unpolarized $\Upsilon(nS)$ ($n = 1, 2, 3$) yields with theoretical predictions obtained using the CASCADE Monte Carlo event generator [59], which is based on a variant of the k_T factorization formalism [13]. In Ref. [59], the $\Upsilon(nS)$ hadroproduction cross sections are adopted from Ref. [60], where they are evaluated in the CS model. The interplay of the lack of CO contributions, the different implementation of k_T factorization, and the inclusion of nonperturbative effects beyond the scope of our analysis, such as parton showering, render a meaningful comparison with our results difficult.

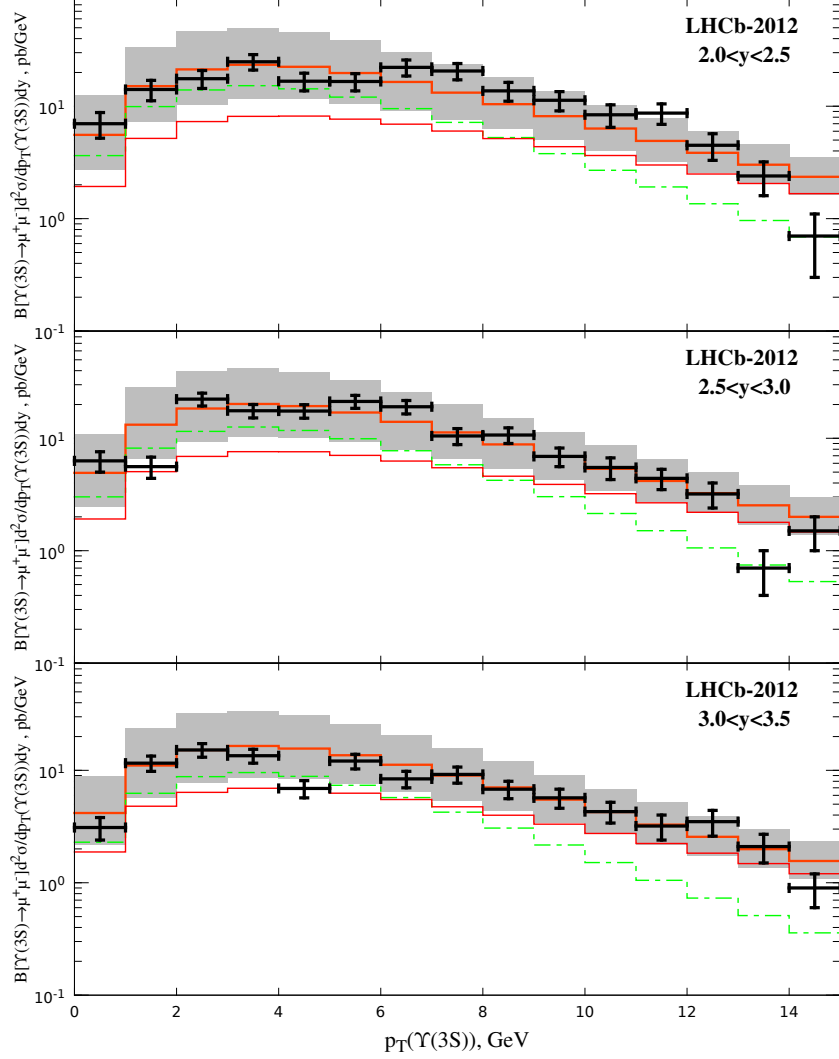


FIG. 9: The LHCb-2012 [41] data sets on the p_T distributions of $\Upsilon(3S)$ inclusive hadroproduction are compared with the predicted LO PRA results in the fusion approximation (thick solid orange histograms) and their theoretical uncertainties (shaded bands). The ${}^3S_1^{(1)}$ (thin dot-dashed green histograms) and ${}^3S_1^{(8)}$ (thin solid red histograms) contributions are shown for comparison. The mixed ${}^1S_0^{(8)}$ and ${}^3P_J^{(8)}$ contribution does not contribute due to $M_R^{\Upsilon(3S)} = 0$ in Table I.

B. Polarization parameters

We now compare the p_T distributions of the polarization parameters λ_θ of $\psi(2S)$ and $\Upsilon(3S)$ mesons measured in the s -channel helicity frame at the Tevatron and the LHC with our LO PRA predictions. As already pointed out in Sec. I, the $\psi(2S)$ and $\Upsilon(3S)$ mesons

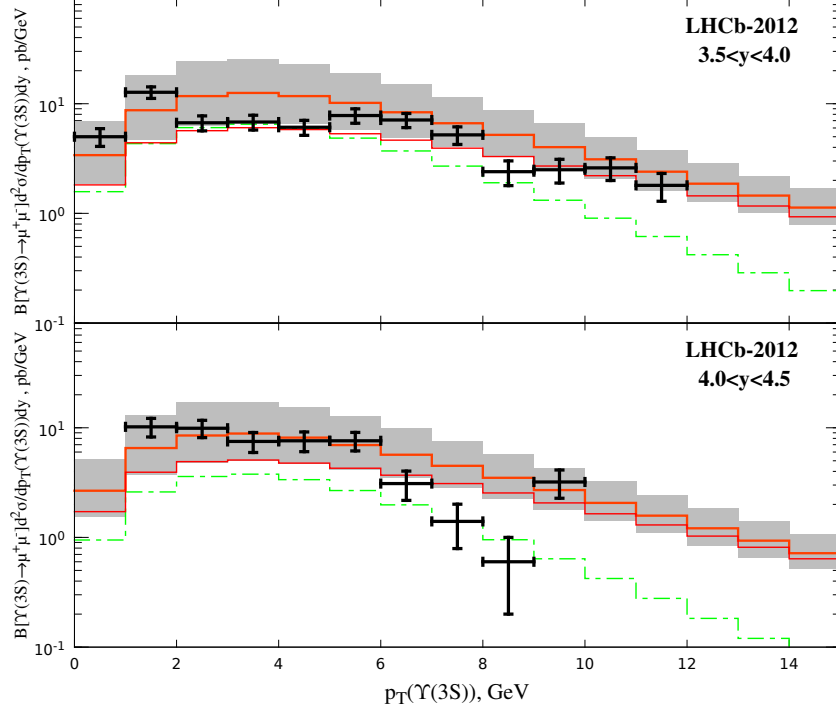


FIG. 10: Figure 9 continued.

allow for particularly pure polarization studies because of the negligible feed-down contributions from charmonia above the $D\bar{D}$ threshold and bottomonia above the $B\bar{B}$ threshold, respectively.

In the $\psi(2S)$ case, we consider the CDF measurement at $\sqrt{S} = 1.96$ TeV in the rapidity bin $|y| < 0.6$ (CDF-2007) [37] and the CMS measurement at $\sqrt{S} = 7$ TeV in the bins $|y| < 0.6$, $0.6 < |y| < 1.2$, and $1.2 < |y| < 1.5$ (CMS-2012) [38]. In the $\Upsilon(3S)$ case, we consider the CDF measurement at $\sqrt{S} = 1.96$ TeV in the bin $|y| < 0.6$ (CDF-2012) [42] and the CMS measurement at $\sqrt{S} = 7$ TeV in the bins $|y| < 0.6$ and $0.6 < |y| < 1.2$ (CMS-2012a) [43]. Our LO PRA predictions are evaluated in the fusion approximation using the respective LDMEs in Table I. The LDME errors dominate because the scale variations largely cancel in the ratio in Eq. (11).

The comparisons for the $\psi(2S)$ and $\Upsilon(3S)$ mesons are shown in Figs. 11 and 12, respectively. From Fig. 11 we observe that the LO PRA predictions tend to overshoot the experimental data [37, 38] at large p_T values. In fact, the $\psi(2S)$ mesons are predicted to be asymptotically transverse, with $\lambda_\theta = 1$, in the large- p_T limit. There, the cross section is practically saturated by the production of the $^3S_1^{(8)}$ state via an almost on-shell gluon, which

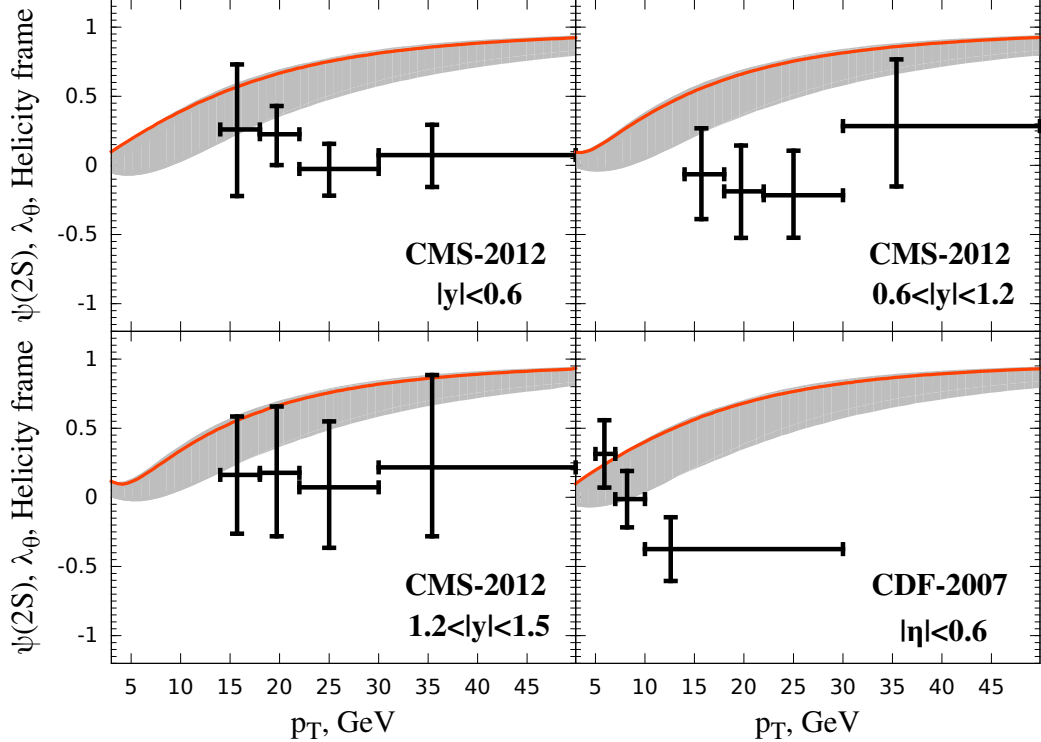


FIG. 11: The CMS-2012 [38] (upper and left lower panels) and CDF-2007 [37] (right lower panel) data sets on the p_T distributions of the $\psi(2S)$ polarization parameter λ_θ in the s -channel helicity frame are compared with the predicted LO PRA results in the fusion approximation (thick solid orange lines) and their theoretical uncertainties (shaded bands).

passes on its transverse polarization via the ${}^3S_1^{(8)}$ state to the $\psi(2S)$ meson. We thus recover the notion charmonium polarization puzzle, which is familiar from the CPM [11, 36].

By contrast, in the $\Upsilon(3S)$ case featured in Fig. 12, there is excellent agreement between the experimental data [42, 43] and our LO PRA predictions, with the exceptions of two CDF-2012 data points. As in the $\psi(2S)$ case, the experimental data are essentially compatible with zero polarization. However, the $g \rightarrow b\bar{b}[{}^3S_1^{(8)}]$ transition does not play a dominant role in the p_T range considered. Similar observations were made at NLO in the CPM [12].

IV. CONCLUSIONS

In the present paper, we studied the hadroproduction of $\psi(2S)$ and $\Upsilon(3S)$ mesons at the Tevatron and the LHC in the NRQCD factorization approach working at LO in the

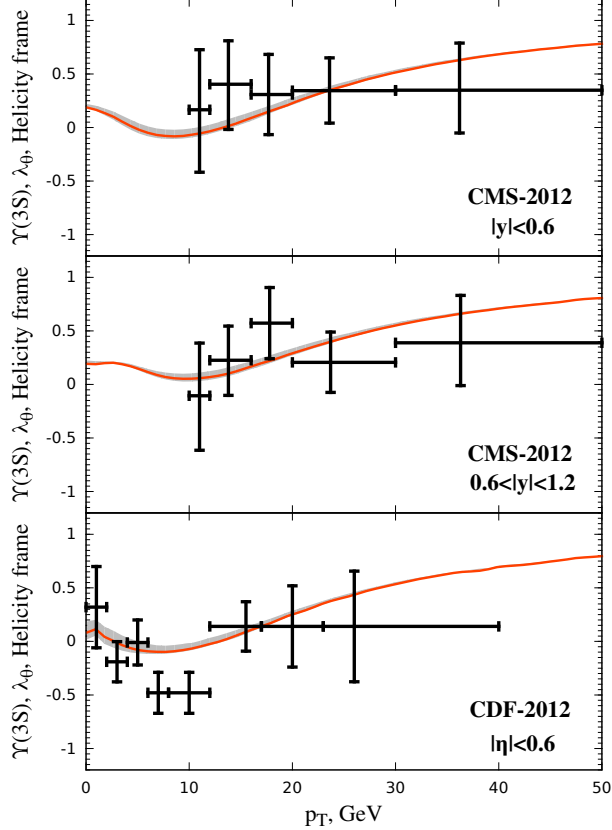


FIG. 12: The CMS-2012a [43] (upmost and center panels) and CDF-2012 [42] (downmost panel) data sets on the p_T distributions of the $\Upsilon(3S)$ polarization parameter λ_θ in the s -channel helicity frame are compared with the predicted LO PRA results in the fusion approximation (thick solid orange lines) and their theoretical uncertainties (shaded bands).

PRA. These are particularly clean probes because the contaminations from feed-down contributions are negligibly small. We considered the unpolarized yields and the polarization parameter λ_θ in the s -channel helicity frame as functions of p_T . While the analytic results for the unpolarized yields are already available in the literature [18], we provided those for λ_θ here.

In the $\psi(2S)$ case, we extracted two sets of CO LDMEs, one by fitting the CDF-2009 [33] data in the fusion approximation and one by jointly fitting the ATLAS-2014 [31] and CMS-2015 [32] data in the fragmentation approximation. We found that the fusion approximation usefully describes the ATLAS-2014 and CMS-2015 data in the lower p_T range, for $p_T \lesssim 30$ GeV, while the fragmentation approximation is indispensable for larger p_T val-

ues. However, we encountered limitations of the PRA at LO in describing the LHCb-2012 [34] measurement in the forward direction. We also verified that the simple kinematic approximation in Eq. (5) leads to a satisfactory description of the CDF-1997 [35] and ATLAS-2014 [31] data on the $p_T^{J/\psi}$ distributions of the J/ψ mesons from $\psi(2S)$ decay. By confronting the CDF-2007 [37] and CMS-2012 [38] data on λ_θ with our predictions in the fusion approximation, we found that the charmonium polarization puzzle, which is familiar from the CPM both at LO [48, 50, 51] and NLO [11], persists at LO in the PRA.

The situation is very different in the $\Upsilon(3S)$ case. Thanks to $M_{\Upsilon(3S)} \gg M_{\psi(2S)}$, the fusion approximation is quite appropriate in the p_T range experimentally accessed so far, and the PRA at LO usefully works also in the forward direction. In fact, the set of CO LDMEs that we fitted to the ATLAS-2013 [40] data yield a nice description of the LHCb-2012a [41] data, albeit the one of the CDF-2002 [39] data is marginal. Furthermore, CDF-2012 [42] and CMS-2012 [38] data on λ_θ agree very well with our LO PRA predictions, which we attributed to the subdominant role of the $g \rightarrow b\bar{b}[{}^3S_1^{(8)}]$ transition.

In conclusion, the PRA once again proved to be a powerful tool for the theoretical description of QCD processes in the high-energy limit. It allows one to achieve useful descriptions of experimental data already at LO in cases when one needs to go to NLO or perform resummations in the CPM. This is in line with our previous studies in the PRA, applied to the production of charmonia [17–21], bottomonia [21–23], D mesons [24], B mesons [25], dijets [26], bottom-flavored jets [27], Drell-Yan lepton pairs [28], monojets, and prompt photons [29, 30]. On the other hand, the PRA at LO fails to solve the charmonium polarization puzzle. Our study indicates that the latter is an intrinsic problem of NRQCD factorization in the final state and rather insensitive to the treatment of gluonic initial-state radiation.

Acknowledgments

The authors are grateful to M. Butenschön for useful discussions and to C. Lourenço for a clarifying communication regarding the CMS-2015 data [32]. The work of B. A. K. was supported in part by the German Federal Ministry for Education and Research BMBWF through Grant No. 05H2015. The work of M. A. N. and V. A. S. was supported in part by the Russian Foundation for Basic Research through Grant No. 14-02-00021 and by the Competitiveness Enhancement Program of Samara University for 2013–2020. The work

of M. A. N. was supported in part by the German Academic Exchange Service DAAD and by the Ministry of Education and Science of the Russian Federation through “Michail Lomonosov” Grant No. A/14/73130 and through Grant No. 1394.

- [1] G. T. Bodwin, E. Braaten, and G. P. Lepage, Phys. Rev. D **51**, 1125 (1995); **55**, 5853(E) (1997) [hep-ph/9407339].
- [2] N. Brambilla *et al.*, Eur. Phys. J. C **71**, 1534 (2011) [arXiv:1010.5827 [hep-ph]]; Eur. Phys. J. C **74**, 2981 (2014) [arXiv:1404.3723 [hep-ph]].
- [3] E. J. Eichten and C. Quigg, Phys. Rev. D **52**, 1726 (1995) [hep-ph/9503356].
- [4] P. Sun, C.-P. Yuan, and F. Yuan, Phys. Rev. D **88**, 054008 (2013) [arXiv:1210.3432 [hep-ph]].
- [5] Y.-Q. Ma and R. Venugopalan, Phys. Rev. Lett. **113**, 192301 (2014) [arXiv:1408.4075 [hep-ph]].
- [6] Z.-B. Kang, Y.-Q. Ma, J.-W. Qiu, and G. Sterman, Phys. Rev. D **91**, 014030 (2015) [arXiv:1411.2456 [hep-ph]]; G. T. Bodwin, K.-T. Chao, H. S. Chung, U.-R. Kim, J. Lee, and Y.-Q. Ma, Phys. Rev. D **93**, 034041 (2016) [arXiv:1509.07904 [hep-ph]].
- [7] M. Butenschön and B. A. Kniehl, Phys. Rev. Lett. **106**, 022003 (2011) [arXiv:1009.5662 [hep-ph]]; Phys. Rev. D **84**, 051501(R) (2011) [arXiv:1105.0820 [hep-ph]].
- [8] Y.-Q. Ma, K. Wang, and K.-T. Chao, Phys. Rev. Lett. **106**, 042002 (2011) [arXiv:1009.3655 [hep-ph]].
- [9] P. Artoisenet, J. Campbell, J. P. Lansberg, F. Maltoni, and F. Tramontano, Phys. Rev. Lett. **101**, 152001 (2008) [arXiv:0806.3282 [hep-ph]].
- [10] M. Butenschön and B. A. Kniehl, Phys. Rev. Lett. **104**, 072001 (2010) [arXiv:0909.2798 [hep-ph]].
- [11] M. Butenschoen and B. A. Kniehl, Phys. Rev. Lett. **108**, 172002 (2012) [arXiv:1201.1872 [hep-ph]]; Mod. Phys. Lett. A **28**, 1350027 (2013) [arXiv:1212.2037 [hep-ph]].
- [12] B. Gong, J.-X. Wang, and H.-F. Zhang, Phys. Rev. D **83**, 114021 (2011) [arXiv:1009.3839 [hep-ph]]; K. Wang, Y.-Q. Ma, and K.-T. Chao, Phys. Rev. D **85**, 114003 (2012) [arXiv:1202.6012 [hep-ph]]; B. Gong, L.-P. Wan, J.-X. Wang, and H.-F. Zhang, Phys. Rev. Lett. **112**, 032001 (2014) [arXiv:1305.0748 [hep-ph]].
- [13] L. V. Gribov, E. M. Levin, and M. G. Ryskin, Phys. Rep. **100**, 1 (1983); S. Catani,

- M. Ciafaloni, and F. Hautmann, Phys. Lett. B **242**, 97 (1990); Nucl. Phys. **B366**, 135 (1991); J. C. Collins and R. K. Ellis, Nucl. Phys. **B360**, 3 (1991).
- [14] L. N. Lipatov, Yad. Fiz. **23**, 642 (1976) [Sov. J. Nucl. Phys. **23**, 338 (1976)]; E. A. Kuraev, L. N. Lipatov, and V. S. Fadin, Zh. Eksp. Teor. Fiz. **71**, 840 (1976) [Sov. Phys. JETP **44**, 443 (1976)]; Zh. Eksp. Teor. Fiz. **72**, 377 (1977) [Sov. Phys. JETP **45**, 199 (1977)]; Ya. Ya. Balitskii and L. N. Lipatov, Yad. Fiz. **28**, 1597 (1978) [Sov. J. Nucl. Phys. **28**, 822 (1978)]; L. N. Lipatov, Zh. Eksp. Teor. Fiz. **90**, 1536 (1986) [Sov. Phys. JETP **63**, 904 (1986)].
- [15] L. N. Lipatov, Nucl. Phys. **B452**, 369 (1995) [hep-ph/9502308]; Phys. Rep. **286**, 131 (1997) [hep-ph/9610276].
- [16] M. A. Kimber, A. D. Martin, and M. G. Ryskin, Eur. Phys. J. C **12**, 655 (2000) [hep-ph/9911379]; Phys. Rev. D **63**, 114027 (2001) [hep-ph/0101348]; G. Watt, A. D. Martin, and M. G. Ryskin, Eur. Phys. J. C **31**, 73 (2003) [hep-ph/0306169]; Phys. Rev. D **70**, 014012 (2004); **70**, 079902(E) (2004) [hep-ph/0309096].
- [17] V. A. Saleev and D. V. Vasin, Yad. Fiz. **68**, 95 (2005) [Phys. Atom. Nucl. **68**, 94 (2005)].
- [18] B. A. Kniehl, D. V. Vasin, and V. A. Saleev, Phys. Rev. D **73**, 074022 (2006) [hep-ph/0602179].
- [19] V. A. Saleev and A. V. Shipilova, Phys. Rev. D **75**, 034012 (2007) [hep-ph/0612217].
- [20] V. A. Saleev, M. A. Nefedov, and A. V. Shipilova, Phys. Rev. D **85**, 074013 (2012) [arXiv:1201.3464 [hep-ph]].
- [21] D. V. Vasin and V. A. Saleev, Phys. Part. Nucl. **38**, 635 (2007).
- [22] B. A. Kniehl, V. A. Saleev, and D. V. Vasin, Phys. Rev. D **74**, 014024 (2006) [hep-ph/0607254].
- [23] M. A. Nefedov, V. A. Saleev, and A. V. Shipilova, Phys. Rev. D **88**, 014003 (2013) [arXiv:1305.7310 [hep-ph]].
- [24] B. A. Kniehl, A. V. Shipilova, and V. A. Saleev, Phys. Rev. D **79**, 034007 (2009) [arXiv:0812.3376 [hep-ph]]; A. V. Karpishkov, M. A. Nefedov, V. A. Saleev, and A. V. Shipilova, Phys. Rev. D **91**, 054009 (2015) [arXiv:1410.7139 [hep-ph]].
- [25] A. V. Karpishkov, M. A. Nefedov, V. A. Saleev, and A. V. Shipilova, Int. J. Mod. Phys. A **30**, 1550023 (2015) [arXiv:1411.7672 [hep-ph]].
- [26] M. A. Nefedov, V. A. Saleev, and A. V. Shipilova, Phys. Rev. D **87**, 094030 (2013) [arXiv:1304.3549 [hep-ph]].
- [27] B. A. Kniehl, V. A. Saleev, and A. V. Shipilova, Phys. Rev. D **81**, 094010 (2010) [arXiv:1003.0346 [hep-ph]]; V. A. Saleev and A. V. Shipilova, Phys. Rev. D **86**, 034032 (2012)

- [arXiv:1201.4640 [hep-ph]].
- [28] M. A. Nefedov, N. N. Nikolaev, and V. A. Saleev, Phys. Rev. D **87**, 014022 (2013) [arXiv:1211.5539 [hep-ph]].
- [29] B. A. Kniehl, V. A. Saleev, A. V. Shipilova, and E. V. Yatsenko, Phys. Rev. D **84**, 074017 (2011) [arXiv:1107.1462 [hep-ph]].
- [30] B. A. Kniehl, M. A. Nefedov, and V. A. Saleev, Phys. Rev. D **89**, 114016 (2014) [arXiv:1404.3513 [hep-ph]].
- [31] G. Aad *et al.* (ATLAS Collaboration), JHEP **1409**, 079 (2014) [arXiv:1407.5532 [hep-ex]].
- [32] V. Khachatryan *et al.* (CMS Collaboration), Phys. Rev. Lett. **114**, 191802 (2015) [arXiv:1502.04155 [hep-ex]].
- [33] T. Aaltonen *et al.* (CDF Collaboration), Phys. Rev. D **80**, 031103(R) (2009) [arXiv:0905.1982 [hep-ex]].
- [34] R. Aaij *et al.* (LHCb Collaboration), Eur. Phys. J. C **72**, 2100 (2012) [arXiv:1204.1258 [hep-ex]].
- [35] F. Abe *et al.* (CDF Collaboration), Phys. Rev. Lett. **79**, 578 (1997).
- [36] H.-S. Shao, H. Han, Y.-Q. Ma, C. Meng, Y.-J. Zhang, and K.-T. Chao, JHEP **1505**, 103 (2015) [arXiv:1411.3300 [hep-ph]].
- [37] A. Abulencia *et al.* (CDF Collaboration), Phys. Rev. Lett. **99**, 132001 (2007) [arXiv:0704.0638 [hep-ex]].
- [38] S. Chatrchyan *et al.* (CMS Collaboration), Phys. Lett. B **727**, 381 (2013) [arXiv:1307.6070 [hep-ex]].
- [39] D. Acosta *et al.* (CDF Collaboration), Phys. Rev. Lett. **88**, 161802 (2002).
- [40] G. Aad *et al.* (ATLAS Collaboration), Phys. Rev. D **87**, 052004 (2013) [arXiv:1211.7255 [hep-ex]].
- [41] R. Aaij *et al.* (LHCb Collaboration), Eur. Phys. J. C **72**, 2025 (2012) [arXiv:1202.6579 [hep-ex]].
- [42] T. Aaltonen *et al.* (CDF Collaboration), Phys. Rev. Lett. **108**, 151802 (2012) [arXiv:1112.1591 [hep-ex]].
- [43] S. Chatrchyan *et al.* (CMS Collaboration), Phys. Rev. Lett. **110**, 081802 (2013) [arXiv:1209.2922 [hep-ex]].
- [44] G. P. Lepage, L. Magnea, C. Nakhleh, U. Magnea, and K. Hornbostel, Phys. Rev. D **46**, 4052

- (1992) [hep-lat/9205007].
- [45] V. N. Gribov and L. N. Lipatov, *Yad. Fiz.* **15**, 781 (1972) [*Sov. J. Nucl. Phys.* **15**, 438 (1972)]; Yu. L. Dokshitzer, *Zh. Eksp. Teor. Fiz.* **73**, 1216 (1977) [*Sov. Phys. JETP* **46**, 641 (1977)]; G. Altarelli and G. Parisi, *Nucl. Phys.* **B126**, 298 (1977).
- [46] A. D. Martin, W. J. Stirling, R. S. Thorne, and G. Watt, *Eur. Phys. J. C* **63**, 189 (2009) [arXiv:0901.0002 [hep-ph]].
- [47] F. Maltoni, M. L. Mangano, and A. Petrelli, *Nucl. Phys.* **B519**, 361 (1998) [hep-ph/9708349].
- [48] M. Beneke, M. Krämer, and M. Vanttinen, *Phys. Rev. D* **57**, 4258 (1998) [hep-ph/9709376].
- [49] P. Faccioli, C. Lourenço, J. Seixas, and H. K. Wöhri, *Eur. Phys. J. C* **69**, 657 (2010) [arXiv:1006.2738 [hep-ph]].
- [50] E. Braaten, B. A. Kniehl, and J. Lee, *Phys. Rev. D* **62**, 094005 (2000) [hep-ph/9911436].
- [51] B. A. Kniehl and J. Lee, *Phys. Rev. D* **62**, 114027 (2000) [hep-ph/0007292].
- [52] P. Cho and A. K. Leibovich, *Phys. Rev. D* **53**, 150 (1996) [hep-ph/9505329]; *Phys. Rev. D* **53**, 6203 (1996) [hep-ph/9511315].
- [53] K. A. Olive *et al.* (Particle Data Group), *Chin. Phys. C* **38**, 090001 (2014).
- [54] M. Butenschoen and B. A. Kniehl, in preparation.
- [55] F. Hautmann and H. Jung, *Nucl. Phys. B* **883**, 1 (2014) [arXiv:1312.7875 [hep-ph]].
- [56] S. Dooling, F. Hautmann, and H. Jung, *Phys. Lett. B* **736**, 293 (2014) [arXiv:1406.2994 [hep-ph]].
- [57] R. Aaij *et al.* (LHCb Collaboration), *Eur. Phys. J. C* **74**, 2872 (2014) [arXiv:1403.1339 [hep-ex]]; B. Abelev *et al.* (ALICE Collaboration), *Eur. Phys. J. C* **74**, 2974 (2014) [arXiv:1403.3648 [nucl-ex]].
- [58] S. Chatrchyan *et al.* (CMS Collaboration), *Phys. Lett. B* **727**, 101 (2013) [arXiv:1303.5900 [hep-ex]].
- [59] H. Jung, S. Baranov, M. Deak, A. Grebenyuk, F. Hautmann, M. Hentschinski, A. Knutsson, M. Krämer, K. Kutak, A. Lipatov, and N. Zotov, *Eur. Phys. J. C* **70**, 1237 (2010) [arXiv:1008.0152 [hep-ph]].
- [60] S. P. Baranov, *Phys. Rev. D* **86**, 054015 (2012).